The Radial Variation of Interplanetary Shocks in the Inner Heliosphere: Observations by *Helios*, MESSENGER, and STEREO

H.R. Lai · C.T. Russell · L.K. Jian · X. Blanco-Cano · B.J. Anderson · J.G. Luhmann · A. Wennmacher

Abstract The two major sources of collisionless shocks in the solar wind are interplanetary coronal mass ejections (ICMEs) and stream interaction regions (SIRs). Previous studies show that some SIR-associated shocks form between Venus and Earth while most form beyond 1 AU. Here we examine the high-resolution magnetometer records from *Helios* 1 and 2 obtained between 0.28 and 1 AU and from MESSENGER obtained between 0.3 and 0.7 AU to further refine our understanding as to where, and in what context, shocks are formed in the inner solar system. From *Helios* data (*Helios* 1 from 1974 to 1981 and *Helios* 2 from 1976 to 1980), we find there were only a few shocks observed inside the orbit of Venus with the closest shock to the Sun at 0.29 AU. We find that there is a strong correlation between shock occurrence and solar activity as measured by the sunspot number. Most of the shocks inside of the orbit of Venus appear to be associated with ICMEs. Even the ICME-associated shocks are quite weak inside the orbit of Venus. By comparing MESSENGER and STEREO results, from 2007 to 2009, we find that in the deep solar minimum, SIR-driven shocks began to form at about 0.4 AU and increased in number with heliocentric distance.

H.R. Lai (✉) · C.T. Russell · L.K. Jian
ESS, UCLA, Los Angeles, CA, USA
e-mail: hlai@igpp.ucla.edu

X. Blanco-Cano
UNAM, México, Mexico

B.J. Anderson
APL, JHU, Laurel, MD, USA

J.G. Luhmann
SSL, UCB, Berkeley, CA, USA

A. Wennmacher
U. Köln, Cologne, Germany

1. Introduction

Interplanetary shocks form across velocity gradients when the change in speed exceeds that of magnetosonic waves. This gradient steepens creating a thin dissipation layer. These collisionless shocks have been studied intensively ever since being discovered. They heat the plasma and accelerate energetic particles (*e.g.* Sarris and Van Allen, 1974). Upstream energetic particles generate waves ahead of the shocks. Russell *et al.* (1983a) found two types of upstream wave: whistler-mode wave and upstream turbulence. The properties of a whistler wave associated to low Mach-number interplanetary shocks were studied by Tsurutani and Smith (1983). Interplanetary shocks are also responsible for geomagnetic effects. Chao and Lepping (1974) found that the sudden compression of the Earth's magnetic field at the time of sudden storm commencements was most often preceded by an interplanetary shock. The two major sources of the interplanetary shocks are interplanetary coronal mass ejections (ICMEs) (Gosling *et al.*, 1975) and stream interaction regions (SIRs).

An ICME is produced by a strong, large-scale magnetic-flux rope initially anchored in the solar corona. During a passage through the center of an ICME, the magnetic field exhibits a coherent rotation over about a day and an increase in magnitude (*e.g.* Hirshberg and Colburn, 1969; Burlaga *et al.*, 1981; Klein and Burlaga, 1982; Gosling, 1990). The plasma density and pressure increase and the plasma temperature decreases (*e.g.* Neugebauer and Goldstein, 1997; Russell and Shinde, 2005). As the velocity of the front of the ejected and expanding rope can be faster than the fast-mode magnetosonic wave speed, the ICME will drive a shock in front of it. Between the rope and the shock, there is a sheath region (McComas *et al.*, 1988), in which the magnetic field and plasma are compressed and disturbed. These properties have been used to inventory ICMEs and study their variations over the solar cycle and with heliocentric-distance (Jian *et al.*, 2006a, 2008a).

SIRs form when fast and slow solar-wind streams originating from different source regions collide (*e.g.* reviewed by Balogh *et al.*, 1999). The fast stream overtakes and compresses the slow one (*e.g.* Smith and Wolfe, 1976). As the magnetized plasma in the two streams cannot interpenetrate, a compression region is created at the interface, pushing forward and backward (Gosling and Pizzo, 1999). During a SIR, the magnetic field and velocity increase; the density and pressure increase inside the slow stream and decrease inside the fast stream. These features have been inventoried by Jian *et al.* (2006b, 2008a and references therein). When the velocity gradient at the front and/or trailing edge of the compression region becomes larger than the fast-mode magnetosonic wave speed, one or two shocks may develop. The shock propagating into the slow stream is a forward shock, moving away from the Sun, while the shock propagating into the fast stream is a reverse shock, moving back toward the Sun. The forward shock accelerates the slow plasma in front of the SIR and the reverse shock decelerates the fast plasma, approaching the SIR from the solar direction.

The strength of a collisionless shock can be measured by its Mach number, the shock speed relative to the upstream plasma divided by the speed of small-amplitude fast-mode magnetosonic waves. In the region beyond 30 solar radii, both gradual and impulsive CMEs reach a speed around 500 km s^{-1} (Sheeley *et al.*, 1999) and often they keep this speed and do not slow down until at large distance from the Sun (*e.g.* Yashiro *et al.*, 2004; Jian *et al.*, 2008b). Near the Sun, the magnetic field is strong and the Alfven speed is high and correspondingly so is the fast-mode speed. Hence even fast CMEs may have difficulty in producing a shock near the Sun. Although ICMEs do slow down as they move away from the Sun, the pressure wave in front of them eventually steepens into a shock because the fast-mode speed drops more rapidly with distance. Similarly, stream interactions are not expected to produce shocks close to the Sun because the interactions are weak there and the

fast-mode velocity is high. They are expected to begin to produce shocks as they approach and pass 1 AU on average (*e.g.* Gosling *et al.*, 1972; Ogilvie, 1972).

Using the *Pioneer Venus Orbiter* (PVO) data, Lindsay *et al.* (1994) found that neither ICME nor SIR disturbances produced many shocks near 0.7 AU, and the most common sources of shocks there were ICMEs. Later Jian *et al.* (2008c) identified the solar-wind structures from 1979 to 1988 at 0.7 AU and found about 48 % of ICMEs drive shocks; while only 3 % of SIRs drive shocks.

To date no examination of high-sample-rate data obtained deeper in the inner solar system has been used to systematically identify shocks. Such high-resolution data can give a more confident identification of shock occurrence than the low-sample-rate data. Recently the high-temporal-resolution data from magnetometers on *MErcury Surface, Space ENvironment, Geochemistry, and Ranging* (MESSENGER) have become available, allowing the study of more interplanetary magnetic structures from 0.3 AU to 0.7 AU. Interplanetary magnetic-field (IMF) data in the same region were recorded by *Helios* 1 and 2 in the 1970s. In this article we examine these records and compare the shock occurrence with *Wind*, *Advanced Composition Explorer* (ACE), and *Solar-TErrestrial RElations Observatory* (STEREO) data to gain further insight as to where, and in what context, shocks are formed in the inner solar system.

2. Data Set and Method

Helios 1 and 2 were launched on 10 December 1974 and 15 January 1976, respectively. They gathered magnetic-field as well as plasma data during Solar Cycle 21. They covered the heliocentric-distance from 0.28 to 1.0 AU. Here we use the *Helios* 1 data from 1974 to 1981 and *Helios* 2 data from 1976 to 1980. The magnetic field is measured by a triaxial fluxgate magnetometer, with a digital resolution of ± 0.2 nT. Its maximum sampling rate is eight vectors per second, but the data are seldom available with a sampling rate greater than 4 Hz (Neubauer *et al.*, 1977). The solar-wind plasma is observed by the plasma analyzer with a best temporal resolution of 40.5 seconds (Rosenbauer *et al.*, 1977). The coverage is best in the early years and varies considerably for the rest of the mission. There are large data gaps especially when the spacecraft passed behind the Sun as seen from the Earth, thus cutting off communication.

MESSENGER was launched on 4 August 2004, but its magnetometer boom was not deployed until 2005, so that the early magnetic-field measurements are contaminated by a strong spacecraft field. Data in 2007 and thereafter are excellent and can be used to search for shocks. They are generally available at 1 Hz and cover the heliocentric-distance from 0.3 to 0.7 AU (Anderson *et al.*, 2007).

Launched on 25 October 2006, the two STEREO spacecraft stay near 1 AU. The magnetic-field data at STEREO are available nominally at 8 Hz and have burst mode at 32 Hz (Acuña *et al.*, 2008); the plasma data have one-minute resolution (Galvin *et al.*, 2008).

Volkmer and Neubauer (1985) found 178 shock waves by examining *Helios* 1 and 2 data from 1975 to 1980. According to their results, shock normals have no heliocentric-distance dependence between 0.3 and 1 AU. Furthermore, they found that 60 % of the shock normals are within 35° of the radial direction. Another result that these authors found is that the magnetohydrodynamic (MHD) Mach numbers lies between one and two and rarely exceed four. However, the authors in that article used an overly simple automatic routine operating on the magnetic field to identify the shocks. Neighboring mean magnetic fields for five minutes are compared. If the angle between the two neighboring mean magnetic fields is

less than 45° and the ratio between the two is either larger than 1.2 or smaller than 0.8 or the magnitude difference between the two is greater than 5 nT, the event is counted as a shock. Using these criteria they might have missed some shocks as well as have counted other structures in the solar wind as interplanetary shocks. Instead, we made our own survey of the *Helios* data while using their shock list as a reference, to ensure that we examine each of their identified intervals carefully.

There is another shock list mentioned in the article by De Lucas *et al.* (2011), which shows 343 shocks from 1974 to 1980, *i.e.* over 50 shocks each year. The authors do not give their criteria to identify the shocks in this article. So we checked the three shock examples shown in their article. Two of the three shocks occur during data gaps in our database. The remaining one is quite weak, but it is still included in our shock list.

When the plasma data of *Helios* 1 and 2 are available, we use them together with the magnetic-field data to identify shocks. We require the following criteria to be satisfied:

 i) The presence of sharp jumps in the magnetic-field magnitude and in at least one magnetic-field component.
 ii) No zero crossings in any of the three components of the magnetic field during the jump.
iii) A density increase when the velocity increases in forward shocks and a drop when the velocity increases in reverse shocks.

Criterion ii) is called the evolutionary condition. Shocks can only compress the magnetic field, but cannot change the direction of the components in the plane of the shock. We find that if one does not include this condition, many directional discontinuities in the solar wind will be classified as shocks. Since the plasma data for *Helios* are often not available or are of poor quality, we determine the typical behavior of the magnetic field when the plasma data are available and apply it to identify shocks when we do not have plasma data.

Jian *et al.* (2006a, 2006b, 2011) have created lists of interplanetary shocks at 1 AU from the data of *Wind*, ACE (from 1995 to 2009), and STEREO (from 2007 to early 2011) (http://www-ssc.igpp.ucla.edu/forms/stereo/stereo_level_3.html). In these lists, based on the magnetic-field and plasma data, the shock origins are also distinguished. We will compare our inner heliosphere shock results with the 1 AU results.

3. Results

In total, 77 shocks are found from *Helios* data (the shock lists can be viewed at: http://www-ssc.igpp.ucla.edu/~hlai/SP11/). Using the *Helios* 1 and 2 plasma data, we are able to determine that 42 shocks are ICME driven, nine are SIR driven, and the remaining 26 are of uncertain origin due to the lack of plasma data. These statistics suggested that if we had plasma data for all shocks, we would likely have found 63 to be ICME driven and 14 to be SIR driven.

Figure 1 shows two different shocks observed near the Sun. From top to bottom are three components and the magnitude of the magnetic field. In this and the later plots the magnetic-field components are all in the shock-coplanarity coordinate system using the standard coplanarity technique (*e.g.* Russell *et al.*, 1983b). In that coordinate system n is the shock normal direction, l is in the shock plane parallel to the projection of the upstream field on the shock, and m completes the right-handed coordinates. As shown in Figure 1, the temporal resolution is low for both cases, because when the spacecraft approached the Sun, the distance became larger for the data transmission. The left shock observed at 0.29 AU is the one closest to the Sun in the *Helios* observations. For this shock, the magnetic
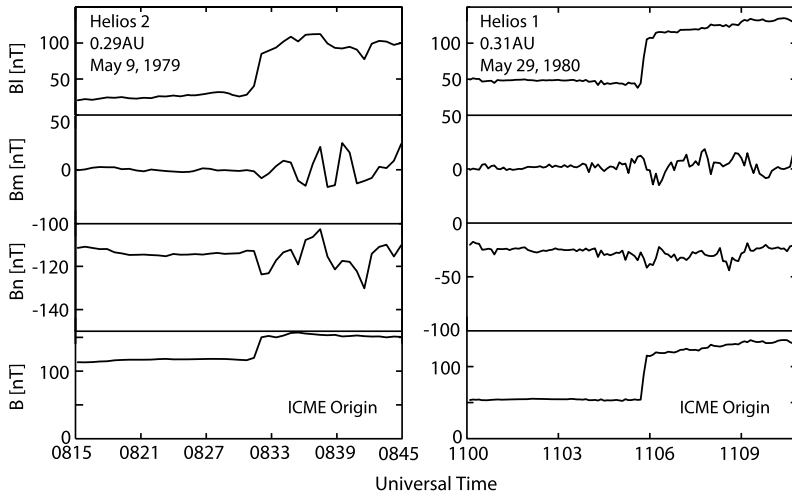
Figure 1 Shocks near the Sun observed by the *Helios* magnetometer. The left shock is the one closest to the Sun, at 0.29 AU, and the shock shown to the right is observed at 0.31 AU. The panels from top to bottom are magnetic-field components and magnetic-field magnitude. The magnetic-field components are in the shock-coplanarity coordinate system, where *n* is the shock normal direction, *l* is in the shock plane parallel to the projection of the upstream field on the shock, and *m* completes the right-handed coordinates. Both of the shocks are ICME driven.

field jumped from 110 nT upstream to 150 nT downstream, a field strength ratio of 1.36. It is a relatively weak shock. However, this does not mean that all near-Sun shocks are weak. In fact, the downstream-to-upstream field ratio is rather constant and varies little with the heliocentric-distance, as we will discuss in detail later. Here we can see another shock example close to Sun on the right, observed at 0.31 AU. It is relatively strong. The magnetic field jumped from 52 nT upstream to 145 nT downstream: a field strength ratio of 2.78. The corresponding plasma data show that both shocks are ICME driven.

Figure 2(a) shows an example of ICME-driven shocks, observed by *Helios* 1 at 0.74 AU. From top to bottom, we show again the three components of magnetic field in the shock-coplanarity coordinate system, the magnetic-field magnitude, total pressure including magnetic pressure and solar-wind plasma thermal pressure [$P_{tot} = nkT + B^2/2\mu_0$], solar-wind velocity, and solar-wind proton number density. We can see that after the jumps in magnetic-field magnitude, in velocity, in density, and in total pressure, as indicated by the first dashed line, the spacecraft entered the sheath region. Inside the sheath, there was turbulence in the magnetic field and solar-wind velocity, and the proton density remained at a high level. Then, as indicated by the second dashed line, the spacecraft entered the flux-rope region. During that time, we can see a smooth rotation in B_m and B_n components, and the magnetic-field magnitude together with total pressure gently decreased. The proton density droped to a low level inside the flux rope. Starting with the shock, including the sheath region and the ejecta, this ICME lasted about 22 hours.

Figure 2(b) shows an example of SIR-driven shocks, observed by *Helios* 1 at 0.98 AU. The plot format is the same as Figure 2(a). After the shock, indicated by the first dashed line, the spacecraft entered the compression region, where the proton density remained at a high level and the total pressure increased. After the total pressure reached its peak, indicated by the second dashed line, the spacecraft entered the fast-stream region, where the solar-wind velocity increased and the proton density droped to a low level. The SIR lasted 22 hours and

Figure 2(a) An ICME-driven shock observed by *Helios* 1 on 1 December 1977 at 0.74 AU. From top to bottom: three components of magnetic field in the shock-coplanarity coordinate system, the magnetic-field magnitude, total pressure including magnetic pressure and solar-wind plasma thermal pressure, solar-wind velocity, and solar-wind proton density. The dashed lines from left to right indicate: the shock, the edge between sheath and flux rope, and the end of the ICME.


(a)
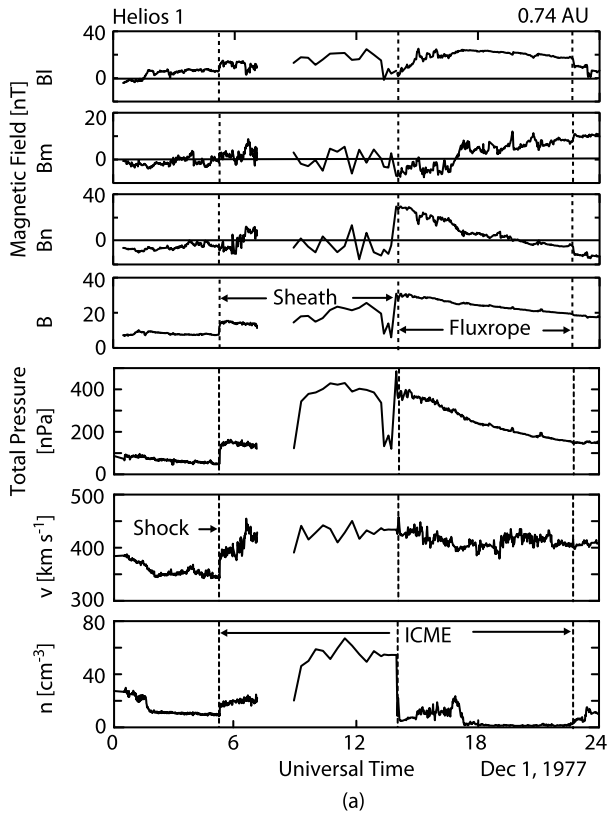
the magnetic field did not rotate smoothly during that time. Also, there was no reverse shock at the end of the SIR in this case.

As *Helios* data cover most of Solar Cycle 21, we can use these observations to determine the relationship between interplanetary-shocks and solar activity. We separate the shocks observed by *Helios* by their origins. The ICME events last from 5.5 to 36 hours and SIRs last from 15 to 60 hours. We then normalize the observed occurrence rate by the observation time. As the database is relatively small, in order to reduce the statistical fluctuation, we use a moving three-point filter with weight (1/4, 1/2, 1/4) for the three successive rates. We plot the total, ICME-driven and SIR-driven annual shock rates from 1974 to 1981 in Figure 3. Also in this figure we show the sunspot number (SSN) in each year filtered the same way as the annual shock rate. From Figure 3, we can see that there is a good correlation between ICME-driven shock occurrence and SSN. In contrast, the SIR-driven shock occurrence has a weak, if any, correlation with SSN. As the SIR-driven shocks maintain their low rate, the ICME-driven shocks dominate and the total shock occurrence rate has a good correlation with SSN. As SSN is a good indicator of the solar activity, Figure 3 shows that ICME-driven shocks are strongly correlated with solar activity while SIR-driven shocks have a weak, if any, correlation. This agrees with the solar-cycle variations of 1 AU shocks over 1995–2009 studied in Jian, Russell, and Luhmann (2011).

In order to understand the radial evolution of interplanetary shocks, we examine the statistical representation of interplanetary-shock occurrence rate as a function of heliocentric-distance. Figure 4 shows the occurrence rates for all shocks observed by *Helios* normalized

Figure 2(b) A SIR-driven shock observed by *Helios* 1 on 2 January 1977 at 0.98 AU. Format is the same as Figure 2(a). The dashed lines from left to right indicate: the shock, the interface between slow stream and fast stream, and the end of the SIR.


(b)
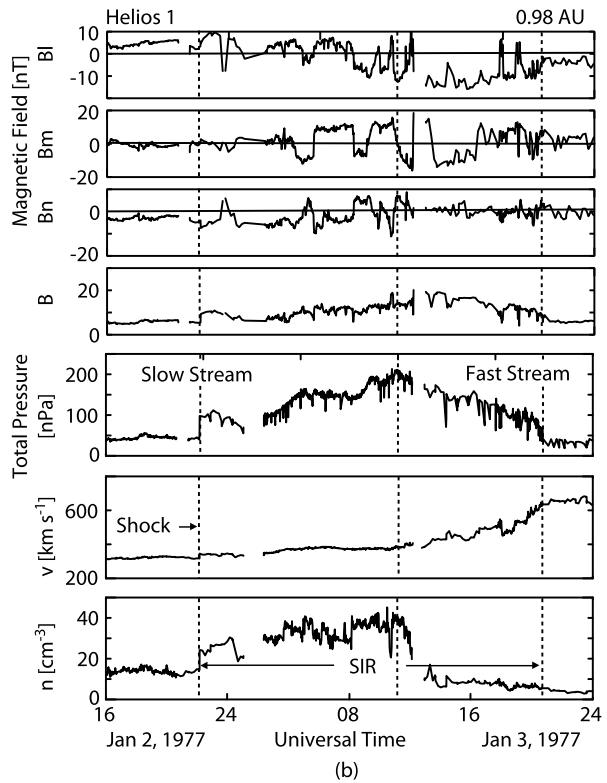
by the observation time in the corresponding range and filtered by the same method as we perform in Figure 3. Also shown here are the 1-AU average and STEREO observations. We use different colors to represent different origins. White indicates an uncertain origin, black is a SIR origin and grey is an ICME origin. Here the 1-AU average is from *Wind* and ACE observations, covering 1995 to 2009. The STEREO data cover from January 2007 to October 2009. From this histogram, we can see that similar to the *Wind* and ACE observations at 1 AU, most shocks in the inner heliosphere are generated by ICMEs and the remaining minor fraction, the SIR-driven shocks, increase in number with heliocentric-distance. Also shown is that there are no clear SIR-driven shocks inside 0.4 AU. The situation is different at STEREO, where the SIR-driven shocks are dominant. This difference is because *Helios* data cover most of a solar cycle, and the *Wind* and ACE number is a 15-year data average and therefore is representative of the whole solar cycle while STEREO was launched into the deepest and longest solar minimum in 200 years (Russell, Luhmann, and Jian, 2010).

As STEREO was launched in such a special solar cycle, it is helpful to measure the radial gradient of shocks contemporaneously with the STEREO data, using MESSENGER cruise data. As stated above, we do not have plasma data from MESSENGER, but we can still distinguish shocks from other solar-wind structures. Figure 5 shows an example of shocks observed by MESSENGER at 0.68 AU. Again the magnetic-field components are in the shock-coplanarity coordinate system. Upstream of this shock, there is wave activity which terminates at the shock. This behavior indicates that these waves are generated at the shock or upstream of it, most probably resonant with energetic particles reflected by, or escaping from, the shock. With all data in hand, we find there are only three shocks in 2008 and one shock

Figure 3 ICME-driven (dotted line), SIR-driven (dashed line), and total shock (solid line) annual occurrence rates and sunspot number (SSN) (dotted-dashed line) from 1974 to 1981. The shock annual rate is normalized by the observation time. The SSN is a good indicator of solar activity. There is a good correlation between ICME-driven shock occurrence and SSN. The SIR-driven shock occurrence has a weak, if any, correlation with SSN. As the ICME-driven shock dominates, the total shock occurrence has a good correlation with SSN.
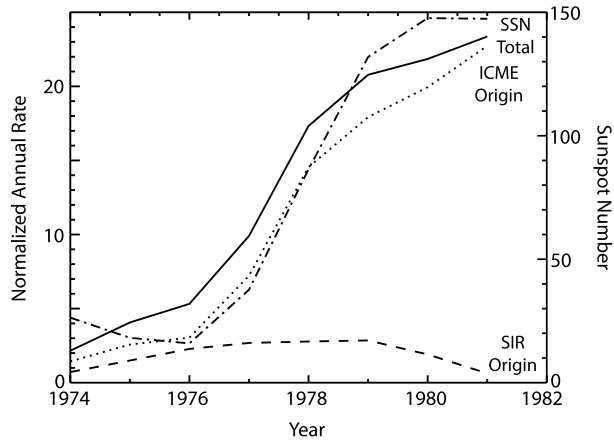

Figure 4 Normalized and smoothed shock annual occurrence rate as a function of heliocentric-distance. *Helios* data cover most of a solar cycle. 1 AU average is based on 15-year *Wind* and ACE data (Jian, Russell, and Luhmann, 2011) and is independent of solar-cycle phase. STEREO data cover from January 2007 to October 2009, the deepest solar minimum. Most shocks in the inner heliosphere are generated by ICMEs. SIR-driven shocks increase in number with heliocentric-distance.
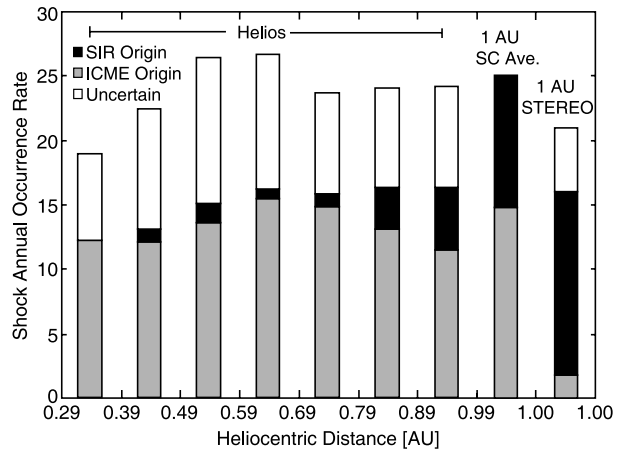

in 2009 observed by MESSENGER and no shocks registered in 2007 (the shock lists can be viewed at: http://www-ssc.igpp.ucla.edu/~hlai/SP11/). As we do not have plasma data for MESSENGER, we cannot determine if these four shocks are ICME or SIR driven from the MESSENGER data. Instead we checked the CME list (http://cdaw.gsfc.nasa.gov/CME_list). With the eruption time and speed at final height, we are able to look for the CME candidates. No CME is found to drive our shocks and the highest speed for all the possible drivers are below 400 km s^{-1}. So we presume that the four shocks are all SIR-driven. We have converted the 2008 observations to an annual rate in three bins and show their correlation with heliocentric-distance in Figure 6. Here we use the same normalizing and filtering methods as we perform in Figure 4. Although the statistical accuracy of these data is low, they are very consistent with the well-determined STEREO SIR-driven shock rates at the same time near 1 AU. It appears that the formation of shocks by SIRs in the inner heliosphere begins at about 0.4 AU and their number grows with distance from the Sun.
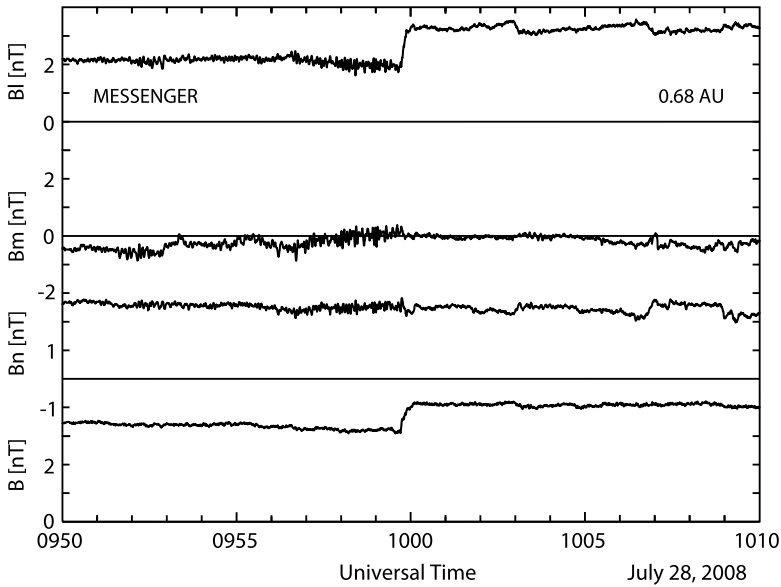
Figure 5 A shock observed by MESSENGER at 0.68 AU. Three components of magnetic field are in the shock-coplanarity coordinate system. There is wave activity in the upstream that terminates at the shock. These waves may originate from cyclotron resonance with reflected or escaping ions upstream of the shock.

Figure 6 Shock annual occurrence rate as a function of heliocentric-distance, MESSENGER *vs.* STEREO observation results. These shocks are observed in the deep solar minimum with little solar activity and no corresponding CMEs were found, so we presume that they are all SIR-driven shocks. It appears that the formation of shocks by SIRs in the inner heliosphere begins at about 0.4 AU and their number grows with distance from the Sun.
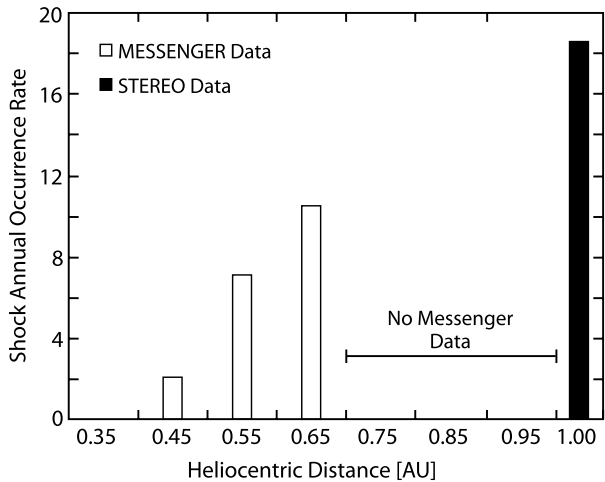
4. Discussion

To compare with Volkmer and Neubauer's (1985) result, we rotate the shocks observed by *Helios* into the shock-coplanarity coordinate system. As 16 of the 77 shocks have only low temporal-resolution data, the shock-normal calculation is not accurate for them. We perform the shock-normal rotation only for the remaining 61 shocks. Lindsay *et al.* (1994) mentioned that nonradial shock normals should result from forward interplanetary shocks produced by SIRs, while interplanetary shocks produced by ICMEs should have more radially oriented

Figure 7 Distribution of cosine of the angle between radial direction and shock normal observed by *Helios*. The occurrence increases as the angle decreases. This is because the ICME-driven shocks, which are more radially aligned, dominate.
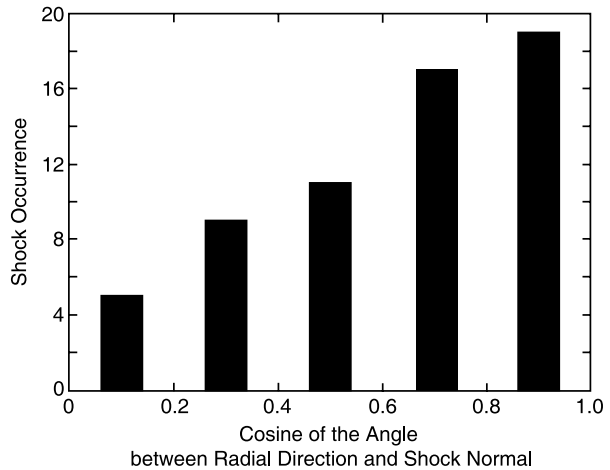

shock normals. In the histogram shown in Figure 7, we plot the shock occurrence as a function of the cosine of the angle between radial direction and shock normal. We can see that the occurrence rate increases as the angle decreases, in agreement with Lindsay *et al.*'s (1994) statement that the ICME-driven shocks dominate in *Helios* observations. However, the angular distribution is not concentrated around 35° (corresponding to 0.82 in cosine) as it is in the work of Volkmer and Neubauer (1985).

Shock strength can give another aspect of the shock evolution in time and space. Mach number is the proper indicator of the shock strength, which is the ratio of the shock speed through the upstream plasma to the fast MHD mode speed. To calculate the Mach number for each shock, we need the plasma data. Although *Helios* has proton data, the resolution is too low for this calculation. So we need to find another indicator of the shock strength. We define the magnetic-field enhancement as the magnetic-field magnitude downstream divided by the field magnitude upstream. It is generally a good indicator, except for quasi-parallel shocks, which have weak field jumps. Also from Rankine–Hugoniot shock theory, the magnetic-field enhancement cannot be larger than four. So it is a nonlinear indicator. The nonlinear effect becomes more obvious when the field enhancement approaches four. But in general, shocks in the inner solar system are sufficiently weak that this is not a problem.

Here we calculate the magnetic-field enhancement for quasi-perpendicular shocks, whose angles between the upstream magnetic field and shock normal are larger than 45°. In total, 50 quasi-perpendicular shocks are found. We show the result as a function of heliocentric-distance in Figure 8. Also shown in this figure is the overlapped median as a solid line, which means we use the median values of a range of 0.2 AU overlapped by 0.1 AU. We can see from the figure that, although for individual shocks the enhancement is quite scattered, the overlapped median stays relatively constant, at about 1.7. Thus we conclude that the correlation between the average magnetic-field jump and heliocentric-distance is weak, despite our expectation that shocks should strengthen with heliocentric-distance. Since new, weak shocks are forming all the way from 0.28 to 1 AU, the median strength remains low. Nevertheless, the older shocks strengthen as they propagate, and the strength of the strongest shocks does increase with distance.

Figure 9 shows an interesting example observed by *Helios* 2. There are two relatively weak shocks in close succession (only six seconds), and the magnetic-field magnitude returns to the value between the two shocks after four minutes. When we see two shocks

Figure 8 Magnetic-field enhancement for quasi-perpendicular shocks as a function of heliocentric-distance. This magnetic-field enhancement is an indicator of shock strength and the solid line shows the overlapped median, which means we use the median values of a range of 0.2 AU overlapped by 0.1 AU. Although the individual points are quite scattered, the overlapped median stays relatively constant. Even though shocks strengthen as they propagate, new weak shocks form all the way from 0.28 to 1 AU, keeping the medians of the magnetic-field enhancement low.
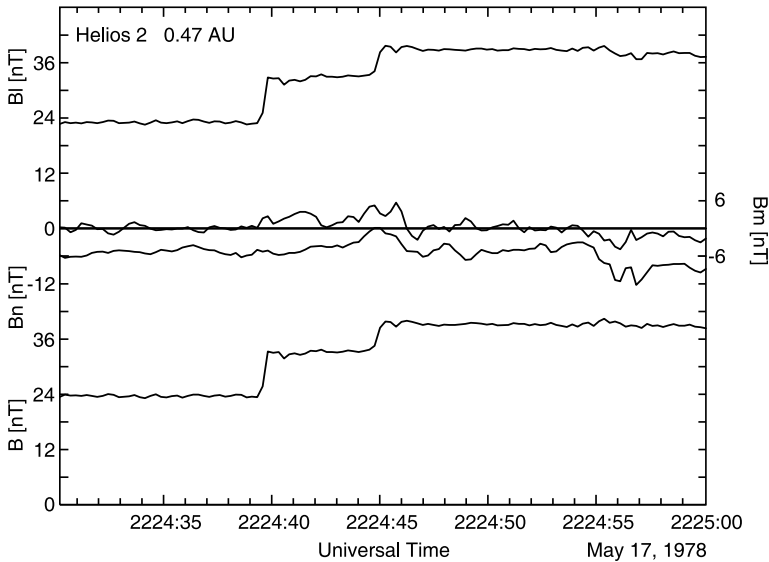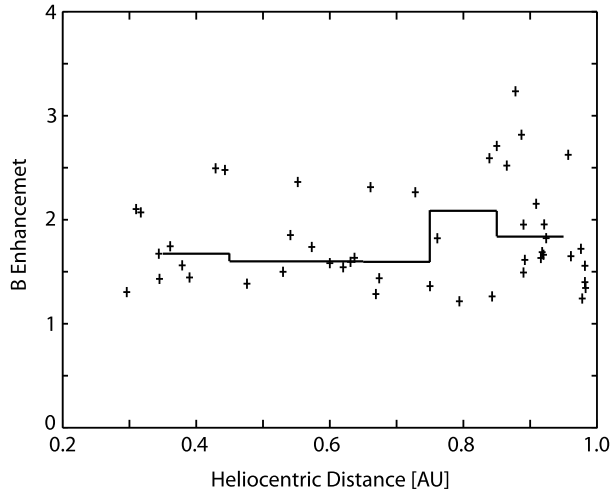
Figure 9 High-resolution *Helios* 2 magnetometer data at 0.47 AU showing two relatively weak shocks in close succession. From top to bottom are three components of magnetic field and magnetic-field magnitude. The magnetic field is in the shock-coplanarity coordinate system. The two shocks will merge into a stronger one with time. These shocks may have formed when a shock encountered a spatial structure in its path that refracted the wave and slowed part of the shock front. Four minutes after the second jump (not shown) the field strength returned to its value seen between the first and second jumps.

following each other closely, we would expect the following one to catch up with the leading one and develop into a stronger single shock at larger heliocentric-distance. In fluid dynamics this phenomenon occurs in tidal bores. Cases of such incipient shock strengthening have been discussed by Russell *et al.* (2009). However, here the shocks are very close in time (an unlikely occurrence). A more likely possibility is that the shock has encoun-

tered a spatially limited high-density region in its propagation that has refracted part of the shock wave, slowing down and strengthening part of the shock front. The slow return of the magnetic-field strength after the second jump to its strength between the two shocks gives support for this scenario.

5. Summary and Conclusion

In order to understand the radial variation of interplanetary shocks and their driving sources, we examine the magnetometer and plasma data of *Helios* 1 from 1974 to 1981 and *Helios* 2 from 1976 to 1980, covering radial distance from 0.28 to 1 AU. To compare with the STEREO observation near 1 AU during the deepest solar minimum since the start of the space age, we also survey the contemporaneous MESSENGER magnetometer data from 2007 to 2009, covering heliocentric-distance from 0.28 to 0.7 AU. We identify 77 shocks from *Helios* observations: 42 driven by ICMEs, 9 by SIRs, and 26 with sources that could not be defined; the closest shock to the Sun was observed at 0.29 AU. There is a strong correlation between shock occurrence and solar activity. Most of the shocks inside 0.7 AU appear to be of ICME origin. From MESSENGER, we find no shock in 2007, three shocks in 2008 and one in 2009. Due to the lack of plasma data, we cannot unambiguously identify the sources of these shocks from the data at the spacecraft alone. As it is in the deepest solar minimum and no corresponding CMEs were found, we suppose that all the shocks are driven by SIRs. Compared with STEREO data at the same time, we find that SIR-driven shocks begin to form at 0.4 AU and their number grows with distance from the Sun. If we use the magnetic-field ratio between upstream and downstream to represent the shock strength of quasi-perpendicular shocks, we find that there is no strong correlation between the shock magnetic-field enhancement and the radial distance, although the maximum shock strength does increase with radial distance.

References

Acuña, M.H., Curtis, D., Scheifele, J.L., Russell, C.T., Schroeder, P., Szabó, A., Luhmann, J.G.: 2008, *Space Sci. Rev.* **136**, 203.
Anderson, B.J., Acuña, M.H., Lohr, D.A., Scheifele, J., Raval, A., Korth, H., Slavin, J.A.: 2007, *Space Sci. Rev.* **131**, 417.
Balogh, A., Gosling, J.T., Jokipii, J.R., Kallenbach, R., Kunow, H. (eds.): 1999, *Space Sci. Rev.* **89**, Kluwer Academic, Dordrecht.
Burlaga, L.F., Sittler, E., Mariani, F., Schwenn, R.: 1981, *J. Geophys. Res.* **86**, 6673.
Chao, J.K., Lepping, R.P.: 1974, *J. Geophys. Res.* **79**, 1799.
De Lucas, A., Schwenn, R., Dal Lago, A., Marsch, E., Clua de Gonzalez, A.L.: 2011, *J. Atmos. Solar-Terr. Phys.* **73**, 1281.
Galvin, A.B., Kistler, L.M., Popecki, M.A., Farrugia, C.J., Simunac, K.D.C., Ellis, L., Möbius, E., Lee, M.A., Boehm, M., Carroll, J., *et al.*: 2008, *Space Sci. Rev.* **136**, 437.
Gosling, J.T.: 1990, In: Russell, C.T., Priest, E.R., Lee, L.C. (eds.) *Geophys. Monogr. Ser.* **58**, AGU, Washington, 343.
Gosling, J.T., Pizzo, V.J.: 1999, *Space Sci. Rev.* **89**, 21.
Gosling, J.T., Hundhausen, A.J., Pizzo, V., Asbridge, J.R.: 1972, *J. Geophys. Res.* **77**, 5442.
Gosling, J.T., Hildner, E., MacQueen, R.M., Munro, R.H., Poland, A.I., Ross, C.L.: 1975, *Solar Phys.* **40**, 439.
Hirshberg, J., Colburn, D.S.: 1969, *Planet. Space Sci.* **17**, 1183.

Jian, L., Russell, C.T., Luhmann, J.G., Skoug, R.M.: 2006a, *Solar Phys.* **239**, 393.

Jian, L., Russell, C.T., Luhmann, J.G., Skoug, R.M.: 2006b, *Solar Phys.* **239**, 337.

Jian, L., Russell, C.T., Luhmann, J.G., Skoug, R.M.: 2008a, *Adv. Space Res.* **41**, 259.

Jian, L.K., Russell, C.T., Luhmann, J.G., Skoug, R.M., Steinberg, J.T.: 2008b, *Solar Phys.* **250**, 375.

Jian, L.K., Russell, C.T., Luhmann, J.G., Skoug, R.M., Steinberg, J.T.: 2008c, *Solar Phys.* **249**, 85.

Jian, L.K., Russell, C.T., Luhmann, J.G.: 2011, *Solar Phys.* **274**, 321.

Klein, L.W., Burlaga, L.F.: 1982, *J. Geophys. Res.* **87**, 613.

Lindsay, G.M., Russell, C.T., Luhmann, J.G., Gazis, P.: 1994, *J. Geophys. Res.* **99**, 11.

McComas, D.J., Gosling, J.T., Winterhalter, D., Smith, E.J.: 1988, *J. Geophys. Res.* **93**, 2519.

Neubauer, F.M., Beinroth, H.J., Barnstorf, H., Dehmel, G.: 1977, *J. Geophys.* **42**, 599.

Neugebauer, M., Goldstein, R.: 1997, In: Crooker, N., Joselyn, J.A., Feynman, J. (eds.) *Coronal Mass Ejections*, *Geophys. Monogr. Ser.* **99**, AGU, Washington, 245.

Ogilvie, K.W.: 1972, In: Coleman, P.J., Sonett, C.P., Wilcox, J.M. (eds.) *Solar Wind*, NASA **SP-308**, Washington, DC, 430.

Rosenbauer, H., Schwenn, R., Marsch, E., Meyer, B., Miggenrieder, H., Montgomery, M.D., Muhlhauser, K.H., Pilipp, W., Voges, W., Zink, S.M.: 1977, *J. Geophys.* **42**, 561.

Russell, C.T., Smith, E.J., Tsurutani, B.T., Gosling, J.T., Bame, S.J.: 1983a, In: Neugebauer, M. (ed.) *Solar Wind Five*, NASA/JPL, 385.

Russell, C.T., Mellott, M.M., Smith, E.J., King, J.H.: 1983b, *J. Geophys. Res.* **88**, 4739.

Russell, C.T., Shinde, A.A.: 2005, *Solar Phys.* **229**, 323.

Russell, C.T., Jian, L.K., Blanco Cano, X., Luhmann, J.G., Zhang, T.L.: 2009, *Geophys. Res. Lett.* **36**, L02103. doi:10.1029/2008GL036337.

Russell, C.T., Luhmann, J.G., Jian, L.K.: 2010, *Rev. Geophys.* **48**, RG2004. doi:10.1029/2009RG00316.

Sarris, E.T., Van Allen, J.A.: 1974, *J. Geophys. Res.* **79**, 4157.

Sheeley, N.R. Jr., Walters, J.H., Wang, Y.M., Howard, R.A.: 1999, *J. Geophys. Res.* **104**, 24739.

Smith, E.J., Wolfe, J.H.: 1976, *Geophys. Res. Lett.* **3**, 137.

Tsurutani, B.T., Smith, E.J.: 1983, *J. Geophys. Res.* **88**, 5645.

Volkmer, P.M., Neubauer, F.M.: 1985, *Ann. Geophys.* **3**, 1.

Yashiro, S., Gopalswamy, N., Michalek, G., St. Cry, O.C., Plunkett, S.P., Rich, N.B., Howard, R.A.: 2004, *J. Geophys. Res.* **109**, A07105. doi:10.1029/2003JA010282.